

Article

# TiO<sub>2</sub>-Based Hybrid Nanocomposites Modified by Phosphonate Molecules as Selective PAH Adsorbents

Nadine Bou Orm <sup>1</sup>, Quoc An Trieu <sup>2</sup> and Stephane Daniele <sup>2,\*</sup>

<sup>1</sup> College of Natural and Health Sciences, Zayed University, 144534 Abu Dhabi, UAE; Nadine.BouOrm@zu.ac.ae

<sup>2</sup> Institut de Recherches sur la Catalyse et l'Environnement de Lyon (IRCELYON), CNRS—UMR 5256, Université de Lyon, 2 Avenue Albert Einstein, F-69626 Villeurbanne CEDEX, France; quoc-an.trieu@ircelyon.univ-lyon1.fr

\* Correspondence: stephane.daniele@ircelyon.univ-lyon1.fr; Tel.: +33-(0)472445360

Academic Editors: Ahmad Mehdi and Sébastien Clément

Received: 25 October 2018; Accepted: 17 November 2018; Published: 21 November 2018



**Abstract:** A robust sol-gel process was developed for the synthesis of surface-functionalized titania nanocrystallites bearing unsaturated groups starting from molecular heteroleptic single-source precursors. Molecules and nanomaterials were thoroughly characterized by multinuclear liquid and solid-state nuclear magnetic resonance (NMR), infra-red (FT-IR, DRIFT) spectroscopies. Nitrogen adsorption-desorption (BET), thermogravimetric (TG) and elemental analyses demonstrated the reliability and the fine tuning of the surface functionalization in terms of ratio TiO<sub>2</sub>:ligand. The as-prepared materials were used as nano-adsorbents to remove mixture of 16 polycyclic aromatic hydrocarbon (PAHs) from aqueous solutions. Adsorption kinetic experiments were carried out for 24 h in solutions of one PAH [benzo(a)pyrene, 220 ppb] and of a mixture of sixteen ones [220 ppb for each PAH]. Most kinetic data best fitted the pseudo-second order model. However, in PAHs mixture, a competition process took place during the first hours leading to a remarkable high selectivity between light and heavy PAHs. This selectivity could be fine-tuned depending on the nature of the unsaturated group of the phosphonate framework and on the nanomaterial textures.

**Keywords:** alkoxides; phosphonates; titania; nanohybrid; sol-gel; PAH adsorption; selectivity

## 1. Introduction

Polycyclic aromatic hydrocarbons (PAHs) are a family of nonpolar neutral chemical compounds resulting from the condensation of several benzene rings ranging from two to three (light molecular weight PAHs, LMW PAHs), to four and five (medium molecular weight PAHs, MMW PAHs) and up to seven (heavy molecular weight PAHs, HMW PAHs). The presence of PAHs in surface water comes mainly from the deposition of airborne particles produced via incomplete oil combustion, from the leaching releases from coal storage areas, from effluents of wood treatment plants and other industries and from the use of composts and fertilizers [1] The number of PAHs identified is in the order of 130, including PAHs containing sulfur, nitrogen or oxygen atoms. The U.S. Environmental Protection Agency (US-EPA) has compiled a list with 16 PAHs (Table S1) posing major environmental problems due to their persistence, their toxic effects on human health and are associated with a wide range of effects: degradation of the immune system, effects on the reproduction and development as endocrine disrupter and carcinogenic properties (carcinogenicity increasing for HMW PAH) [2].

PAHs are persistent pollutants in the environment since they are often resistant to biodegradation. Their removal using conventional physical and/or chemical technologies available for remediation of wastewater pollutants such as oxidation with ozone/hydrogen peroxide, photocatalytic degradation,

ion exchange, membrane (ultra)filtration, coagulation/flocculation, solvent extraction and reverse osmosis can also be not efficient. However, solid-phase extraction is generally considered to be superior for water re-use in terms of energy costs, flexibility and simplicity of design, ease of operation and insensitivity to toxic pollutants and because it does not result in the formation of harmful by-product or toxic concentrated sludge [3–5].

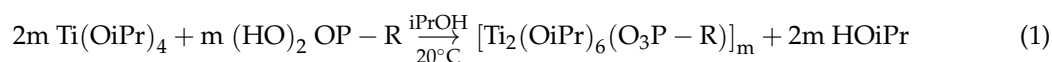
Hybrid (organic-inorganic) nanostructured materials of class II combining large surface-to-volume ratio and controllable surface functionalization can provide a powerful potential to update traditional adsorption treatment process. One of the goals of nanotechnology for the pollutant removal from wastewater is to develop efficient and selective nanosorbents that can remove low concentration contaminants in the presence of competing ones. A recent study on the removal selectivity of PAHs from a wastewater treatment plant (WWTP) located in an urban area in China shows that LMW PAHs such as naphthalene can be removed at a level of 80%, while HMW ones became even more concentrated with treatment in both the dissolved phase and the dewatered sludge [6]. Given the nature of PAHs, use of supported-aromatic derivatives to form " $\pi$ -stacking" charge transfer complexes has already been reported since these interactions are effective in an aqueous medium, non-degrading and reversible [7–9]. Previous studies have reported the removal of PAHs from aqueous solutions using a large variety of supports such as clay, resins, activated carbon, periodic modified mesoporous organosilane (POMs), metal-organic frameworks (MOFs) [4,5,10]. However, studies dealing with the influence of the nature of the trapping organic molecule on adsorption properties towards PAH selectivity or affinity in mixture of LMW and HMW ones are scarce.

In this study, we report the synthesis, characterization and properties of new hybrid (in this case organic-inorganic) nanotitania supports functionalized with a series of organophosphorus molecules (R–OPO<sub>2</sub>H<sub>2</sub>) holding different unsaturated groups (R = vinyl, phenyl, naphthyl) and spacers. The performances of such  $\pi$ -stacking complexation sites will be compared in terms of selectivity, capacity and kinetic of adsorption in an aqueous mixture of 16 PAH molecules. There is an abundant literature reporting the use of organophosphorus molecules for surface modification of metal oxides (MO<sub>x</sub>) because they allow the control of a mono-layer functionalization of metal oxide surfaces resulting from the non-competition between hetero- and homo-condensation but also but also because this ionocovalent anchoring is highly stable through multiple M–O–P bonds [11,12]. In particular, the Titanium oxide will be our nano-support of choice, because of the simple "soft chemistry" preparation routes of crystallized nanoparticles of titanium oxide widely studied in the literature and in our laboratory [13].

## 2. Results and Discussion

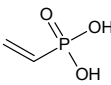
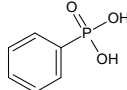
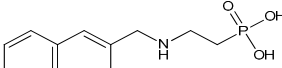
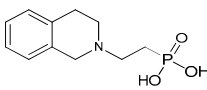
### 2.1. Heteroleptic Precursors Synthesis

A series of heteroleptic phosphonate derivatives of general formulae [Ti<sub>2</sub>(OiPr)<sub>6</sub>(O<sub>3</sub>P–R)]<sub>m</sub> [R = C<sub>2</sub>H<sub>3</sub> (1), C<sub>6</sub>H<sub>5</sub> (2), CH<sub>2</sub>CH<sub>2</sub>NHCH<sub>2</sub>(C<sub>10</sub>H<sub>7</sub>) (3), CH<sub>2</sub>CH<sub>2</sub>(NC<sub>9</sub>H<sub>10</sub>) (4)] was synthesized by Brönsted acid-base reactions between Ti(OiPr)<sub>4</sub> and 0.5 equivalents of the corresponding phosphonic acid (Table 1), at ambient temperature in isopropanol and under an argon atmosphere (Equation (1)).



Higher equivalents of phosphonic acid led to insoluble precipitates. After a drying process, all products were orange-brown liquids. Compounds 1 and 2 were soluble in THF while 3 and 4 were only soluble in hot isopropanol.

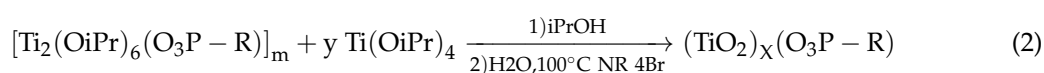
**Table 1.** Structures of the different phosphonic acids used in this study.

Different Phosphonic Acids	Structures
Vinyl phosphonic acid (VPA)	
Phenyl phosphonic acid (PPA)	
(2-[(Naphthalen-2-yl) methyl] amino) ethyl phosphonic acid (NMAPA)	
[2-(3,4-Dihydroisoquinolin-2(1H)-yl) ethyl]phosphonic acid (HQPA)	

All the derivatives were obtained in quantitative yields without purification step and were fully characterized by FT-IR, <sup>1</sup>H- and <sup>31</sup>P-NMR and P, Ti elemental analyses. All FT-IR spectra exhibited absorption bands at 1260 cm<sup>-1</sup>, between 1200 and 950 cm<sup>-1</sup> and below 800 cm<sup>-1</sup> corresponding to P=O, P-O and Ti-O bonds, respectively. The <sup>1</sup>H-NMR spectrum of **1**, at room temperature in CDCl<sub>3</sub>, displayed a 36:6:3 relative integration between CH<sub>3</sub>, CH and vinylic, respectively, in agreement with the proposed general formulae [Ti<sub>2</sub>(OiPr)<sub>6</sub>(O<sub>3</sub>PC<sub>2</sub>H<sub>3</sub>)<sub>m</sub>]. The <sup>31</sup>P-NMR spectrum showed the presence of only a single signal at 7.46 ppm, high fielded in comparison to the vinyl phosphonic acid at 18.88 ppm. Same characteristics were observed for all the derivatives **2–4** and were in agreement with the literature data [11].

## 2.2. Hybrid Nanomaterials Synthesis

Derivatives **1–4** have been used as hydrolysable precursors in a further sol-gel step to afford hybrid (TiO<sub>2</sub>)<sub>x</sub>(O<sub>3</sub>P-R) nanomaterials, following a procedure we have already described for titania carboxylic surface modification [14] (Equation (2)). By varying the co-hydrolysis step parameters, we have checked the influence of the amount and/or the nature of R moiety towards the performance of the resulting nanomaterials as nano-absorbents for a mixture of 16 PAHs.



### 2.2.1. Syntheses and Characterization of (TiO<sub>2</sub>)<sub>x</sub>(VPA) Samples (Ti/P ratio (x) = 2–200)

The first parameter to modify was the amount of vinyl phosphonic acid (VPA) by co-hydrolyzing the derivative **1** with different amounts of Ti(OiPr)<sub>4</sub> in order to produce white powders with controlled Ti/P ratio (x) from 2 to 200. All X-ray powder diffractograms corresponded to the anatase phase of TiO<sub>2</sub> (file ICDD PDF-4+, 00-21-1272) with crystallite sizes estimated by the Debye-Scherrer equation at around 4–6 nm in size (Figure S1). This result suggested that the crystallite size of TiO<sub>2</sub>, the nature of the phase and the crystallinity were not affected by the presence of the phosphonic acid graft up to a certain limit, since the highest concentrated phosphonic acid sample (x = 2) was amorphous. Unlike pure TiO<sub>2</sub>, no trace of the brookite phase was detected.

Figure 1 shows the nitrogen adsorption-desorption isotherms for the bare TiO<sub>2</sub> and some samples (TiO<sub>2</sub>)<sub>x</sub>(VPA) (x = 50, 100, 200) desorbed at 100 °C for 6 h. All displayed type IV(a) isotherms with an H2(b)-type hysteresis loop (according to IUPAC terminology) [15], typical for mesoporous materials with complex pore-networks. Data showed a slight increase of the specific surface area up to 269–333 m<sup>2</sup>/g for hybrid samples and that these latter exhibited larger final saturation plateau than bare TiO<sub>2</sub>, suggesting higher inter-particle interactions and extra-mesoporosity.

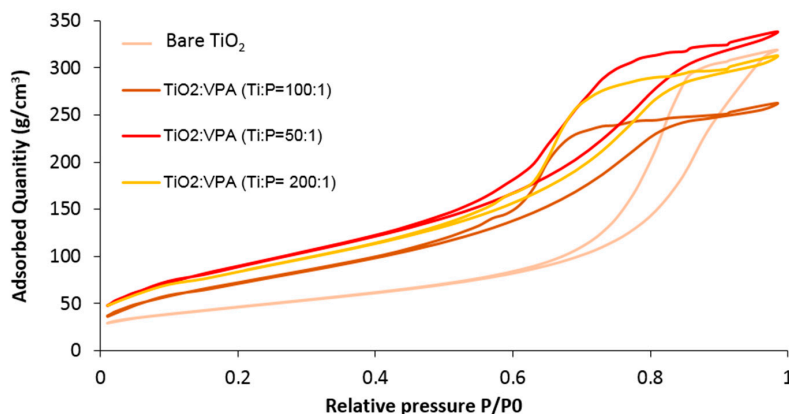


**Figure 1.**  $N_2$  adsorption-desorption isotherms for bare  $TiO_2$ , and hybrid samples  $(TiO_2)_x(VPA)$  with  $x = 50, 100$  and  $200$ .

The most important study remained the surface characterizations in order to compare the different sample natures and to correlate them to the synthesis procedure and to their final properties as PAH nano-absorbents.

All FT-IR spectra exhibited strong absorption bands ascribed to Ti-O and O-H bonds below  $800\text{ cm}^{-1}$ , around  $1620\text{ cm}^{-1}$  and above  $2800\text{ cm}^{-1}$ , (Figure S2), however, the concentrations of VPA were too small to display clear absorption bands assigned to O-P-O group between  $1200$  and  $950\text{ cm}^{-1}$ . Only a weak band at  $1260\text{ cm}^{-1}$  was related to P=O bond. Phosphonate and C=C bonds were evidenced by DRIFT experiments under argon at  $150\text{ }^\circ\text{C}$  since spectra displayed strong adsorption bands at around  $1000\text{ cm}^{-1}$  (symmetrical and unsymmetrical stretching band of O-P-O) and weak ones at  $1260\text{ cm}^{-1}$  ( $\nu\text{P=O}$ ), and  $1619\text{ cm}^{-1}$  ( $\nu\text{C=C}$ ). (Figure 2) Absorption bands in the range of  $3000\text{--}2800\text{ cm}^{-1}$  (C-H bending) and  $1500\text{--}1350\text{ cm}^{-1}$  (C-H stretching) could be explained by the presence of residual alcohol molecules at the surface.

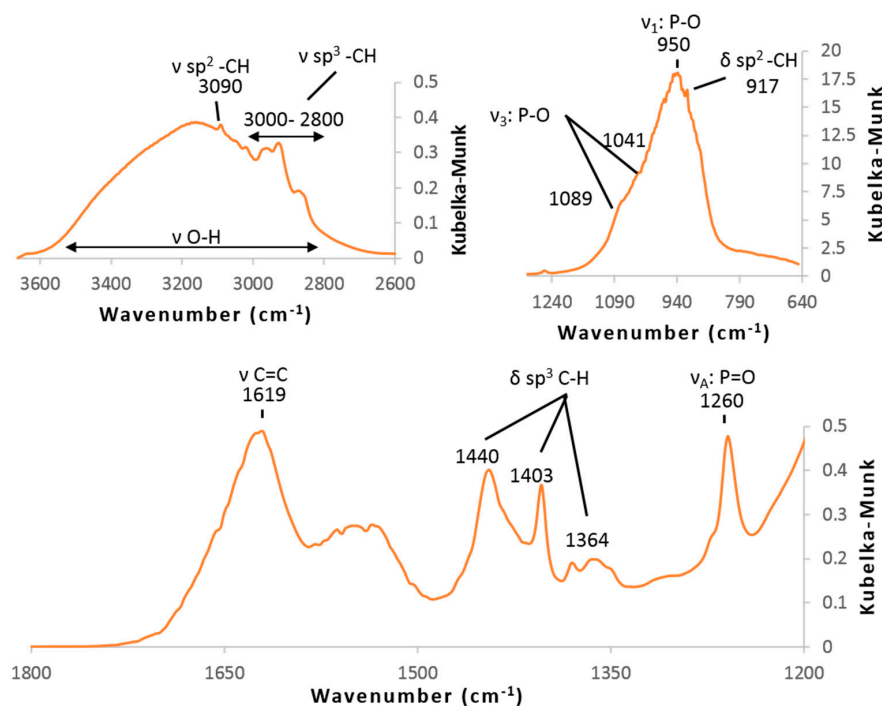


**Figure 2.** DRIFT spectra of samples  $(TiO_2)_{100}(VPA)$  at  $150\text{ }^\circ\text{C}$ .

In an attempt to quantify the final VPA content or at least to estimate its control, TGA-TDA experiments of the  $(TiO_2)_x(VPA)$  samples were performed under air from  $20$  to  $600\text{ }^\circ\text{C}$ . All the patterns

were similar and displayed two major weight losses ranging from 20 to 170 °C (endothermic step) and from 170 to 500 °C (exothermic step), corresponding to the removal of water and solvents (alcohols) adsorbed and to the pyrolysis the hydroxyl groups (–OH) and surface vinyl phosphonates, respectively (Figure S3). The relationship between the organic content and the weight loss observed in TGA was difficult to establish since phosphate ligands ( $\text{PO}_4$ ) still remained onto the  $\text{TiO}_2$  surface until 900 °C.

However, in comparison with the TDA patterns of the richest VPA sample (from the hydrolysis of **1**) and the bare  $\text{TiO}_2$ , one could estimate that the removal of vinyl phosphonic organic units occurred mainly between 300 and 450 °C. The increase in the organic content at the surface was also accompanied by a reduction in the intensity of the TDA peak between 200 and 275 °C, associated to the loss of –OH groups (Figure 3).

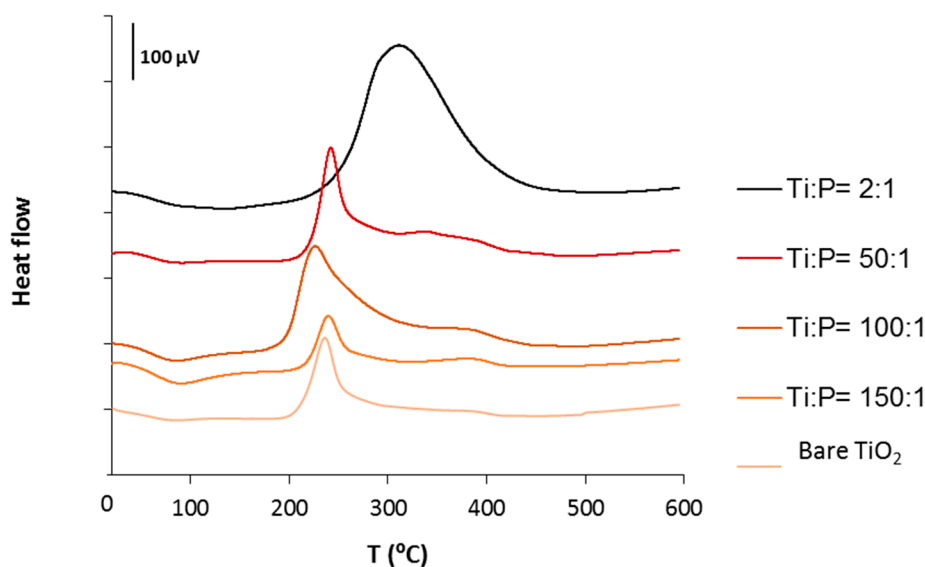


**Figure 3.** TDA of bare and some hybrid  $\text{TiO}_2$  samples (samples  $\text{Ti}/\text{P} = 25; 75, 125$  and  $200$  are omitted for clarity).

Then, by plotting the weight loss between 300 and 500 °C versus the starting  $\text{Ti}/\text{P}$  ratios (Figure 4), one could demonstrate that weight losses followed a linear trend ( $y = -0.0189x + 4.5638$ ) with a high regression coefficient  $R^2 = 0.94$ .

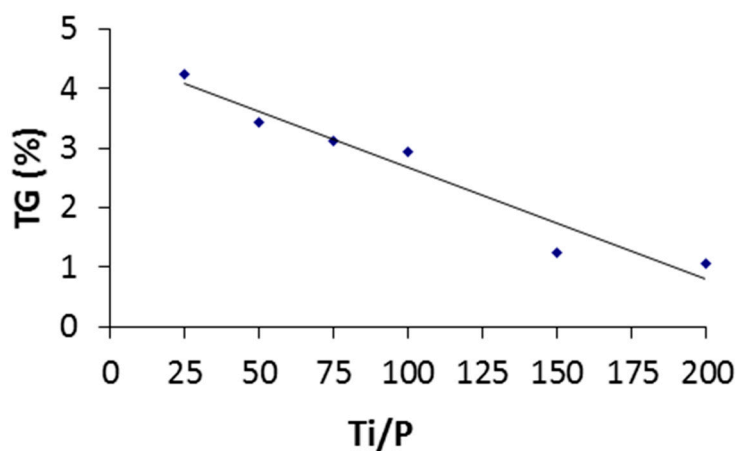


**Figure 4.** Variation of organic weight loss in the range of 300–500 °C in thermogravimetric analysis as a function of the starting  $\text{Ti}/\text{P}$  ratio.

The most loaded sample ( $\text{Ti}/\text{P} = 25$ ) having the highest weight loss of 4.25%, while for higher  $\text{Ti}/\text{P}$  ratios, a phenomenon of dilution of the phosphonate ligands at the  $\text{TiO}_2$  surface logically decreased

the percentages down to 1.05%. Such thermal analysis has thus demonstrated that the phosphonate loading in the hybrid nanomaterial has varied constantly with the initial stoichiometry of the solutions of hydrolysis (Ti/P ratio) and therefore, the degree of surface functionalization of TiO<sub>2</sub> nanocrystallites could be controlled, to some extent, by the initial concentration of the heteroleptic precursor holding the phosphonate moiety. Ti and P elemental analyses on the samples (TiO<sub>2</sub>)<sub>x</sub>(VPA) were carried out and exhibited close values to the expected ones (Table 2).

**Table 2.** Ti and P elemental analyses of the samples (TiO<sub>2</sub>)<sub>x</sub>(VPA).

Theoretical Ti/P Ratio	Experimental		
	% Ti	% P	Ti/P Ratio
25	50.69	1.03	32
50	51.29	0.72	46
75	82.00	0.82	65
100	50.03	0.35	92
125	68.43	0.36	123
150	79.84	0.35	148
200	106.31	0.36	190

<sup>31</sup>P {<sup>1</sup>H} MAS NMR experiments exhibited similar patterns show two distinct resonances upfield and downfield shifts (lower and higher ppm) at about 19 and 13 ppm and broadened compared to the resonance of the original ligand VPA at about 18 ppm (Figure S4). These data, in agreement with the data given in the literature, did again confirm the phosphonate grafting onto the TiO<sub>2</sub> surface nanoparticles [16,17]. The width of the peaks and the presence of P=O absorption band in DRIFT spectra (Figure 2) suggested a mixture of bidentate and tridentate surface grafting modes [11]. The data also demonstrated the absence of molecular titanium phosphonate phases formed by dissolution-precipitation process which are expected to give peak at higher field such as layered titanium phenyl-phosphonates at −4.0 ppm [18].

In an attempt to choose an appropriate Ti/P ratio for the following adsorption study, we estimated the density of VPA molecules onto 5 nm TiO<sub>2</sub> nanocrystallite surface. The intermediate Ti/P ratio of 100 was selected for comparison because (i) sample contained enough phosphonic acid ligand to show an effect and (ii) only 12% of Ti atoms were coordinated or 5 % of the surface were covered, assuming only tridentate bonding mode or an area of 24 Å<sup>2</sup> per molecule of phosphonic acid, respectively. This would achieve high dispersion of the un-saturated receptor, avoiding any side π–π stacking effect between aromatic rings onto the surface. In the same way, Stellaci et al. have demonstrated the use of mixed-ligand gold-coated nanoparticles (short and long thioethers) as efficient receptor for PAH because of supramolecular effect [19]. So for the following syntheses, the theoretical ratio Ti/P was kept constant to 100.

### 2.2.2. Syntheses and Characterizations of (TiO<sub>2</sub>)<sub>100</sub>(O<sub>3</sub>P-R) Samples

Following the same procedure as for the VPA ligand, a series of three new hybrid nanomaterials of general formulae (TiO<sub>2</sub>)<sub>100</sub>(O<sub>3</sub>P-R) was synthesized as white powders. The elemental analyses data confirmed a Ti/P ratio close to 100 (Table 3).

**Table 3.** Ti and P elemental analysis of hybrid samples (TiO<sub>2</sub>)<sub>100</sub>(O<sub>3</sub>P-R).

R Group	PPA	NMAPA	HQPA
% Ti	54.52	59.62	59.06
% P	0.36	0.36	0.36
Ti/P	98	106	105

Powder XRD (Figure S5), FT-IR (Figure S6), TGA-TDA (Figure S7) and solid state  $^{31}\text{P}$   $\{^1\text{H}\}$  MAS NMR (Figure S8) data were consistent with the results already obtained with the VPA ligand. In addition, nanomaterials belonging aromatic rings such as  $(\text{TiO}_2)_{100}(\text{PPA})$ ,  $(\text{TiO}_2)_{100}(\text{NMAPA})$ , and  $(\text{TiO}_2)_{100}(\text{HQPA})$ , displayed a characteristic shift of the carbons linked to the aromatic ring at  $\delta = 128$  ppm in the solid state  $^{13}\text{C}$   $\{^1\text{H}\}$  MAS NMR spectra (Figure S9).

Similar to VPA-based hybrid nanomaterials, the three new hybrid nanomaterials exhibited close specific surface area ( $225\text{--}322\text{ m}^2/\text{g}$ ) and volume pore ( $0.39\text{--}0.51\text{ cm}^3/\text{g}$ ) and similar type IV(a) isotherms than bare  $\text{TiO}_2$  (Figure 5 and Table S2). However,  $(\text{TiO}_2)_{100}(\text{PPA})$  and  $(\text{TiO}_2)_{100}(\text{NMAPA})$  materials displayed different adsorbent textures with type H3 hysteresis loops suggesting the presence of macroporosity [20].

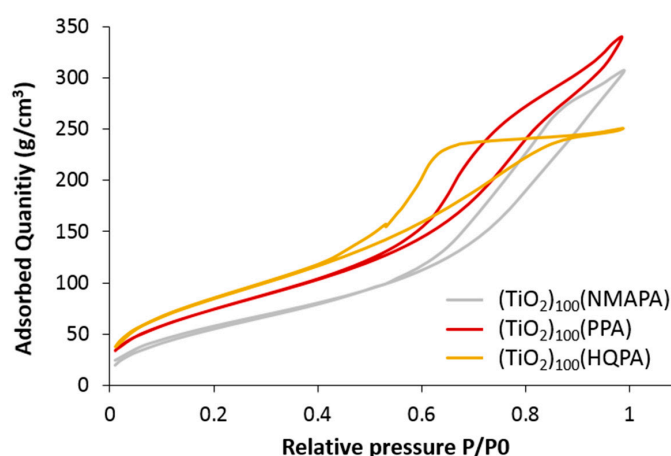


**Figure 5.** Nitrogen adsorption-desorption isotherms of  $(\text{TiO}_2)_{100}(\text{PPA})$ ,  $(\text{TiO}_2)_{100}(\text{NMAPA})$ ,  $(\text{TiO}_2)_{100}(\text{HQPA})$ .

### 2.3. Kinetic PAH Adsorption Studies of $(\text{TiO}_2)_{100}(\text{O}_3\text{P-R})$ Samples

Batch absorption tests using 10 mg of  $(\text{TiO}_2)_{100}(\text{VPA})$  and 50 mL of 200 ppb PAH aqueous solution for 24 h at  $20\text{ }^\circ\text{C}$  and at pH 6.5, showed that the 16 PAH molecules were extracted with efficiencies of 93–100% leading to a high total equilibrium adsorption capacity of around  $16\text{--}17\text{ mg}\cdot\text{g}^{-1}$  (or around  $1\text{ mg}\cdot\text{g}^{-1}$  of each PAH). This was confirmed by doubling the volume of PAH aqueous solution, using 100 mL batches of 200 ppb PAH solution with 10 mg of the materials, whereupon the adsorption percentage was half that of the previous tests (Figure 6).

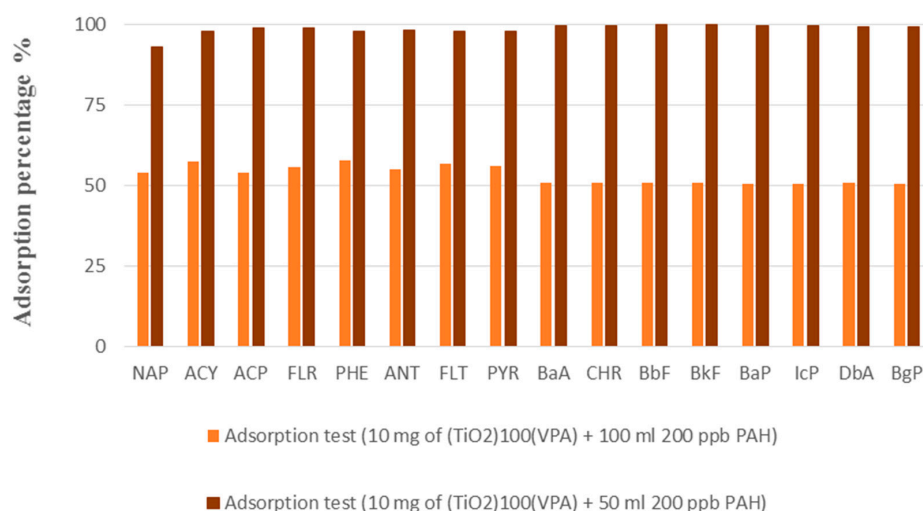


**Figure 6.** Batch adsorption tests of  $(\text{TiO}_2)_{100}(\text{VPA})$  after 24 h.

Close values were reported for nano-hybrids  $\text{NH}_2\text{-SBA-15}$  towards three PAHs (naphthalene, acenaphthylene and phenanthrene) [22] and periodic mesoporous organosilica functionalized with phenyl groups towards a mixture of five PAHs (naphthalene, acenaphthene, fluorine, fluoranthene, pyrene) [23] with adsorption capacity ranges of  $0.76\text{--}1.92\text{ mg g}^{-1}$  and  $0.72\text{--}1.69\text{ mg g}^{-1}$ , respectively. Nano-adsorbents combining both  $-\text{NH}_2$  and phenyl groups such as hybrid mesoporous *p*-aminobenzoic acid-MCM-41 (PABA-MCM-41) nano-materials were used to remove benzo[k]fluoranthene and benzo[b]fluoranthene from aqueous media [200 ppb] and have exhibited lower adsorption capacity in the range of  $23\text{--}27\text{ }\mu\text{g g}^{-1}$  [24].

Adsorption kinetics studies were then carried out to determine the time required to reach adsorption equilibrium, the extraction efficiencies and the selectivities towards the PAHs of the different hybrid sorption systems.

We carried out the experiment with  $(\text{TiO}_2)_{100}(\text{VPA})$  in an aqueous solution containing only one PAH [i.e. benzo(a)pyrene] at a concentration of 220 ppb. The pattern showed that the equilibrium was reached after 90 min leading to an equilibrium capacity of  $0.97\text{ mg}\cdot\text{g}^{-1}$ . Figure 7 showed that experimental data fitted very well with the pseudo-second order model ( $R^2$  value of 1.0000) (Table S3) as largely reported for other adsorbents such as zeolite, clays, sepiolite, activated carbon, biosorbents and hybrid mesoporous material [5]. Thanks to high surface area of  $(\text{TiO}_2)_{100}(\text{VPA})$  nano-materials and stirring during the adsorption, mass transfer process of adsorbates to nano- $\text{TiO}_2$ 's surface was negligible that left interaction between adsorbates and active site on surface of adsorbent and adsorbate as a rate-limiting step in the adsorption process.

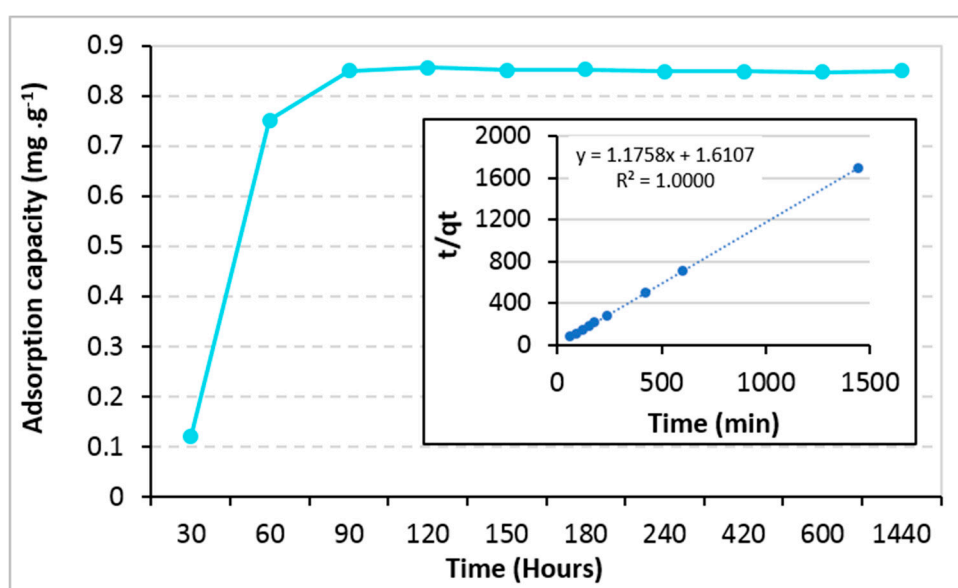


**Figure 7.** Adsorption capacity of  $(\text{TiO}_2)_{100}(\text{VPA})$  toward benzo(a)pyrene as a function of time. Insert: Pseudo-second model for benzo(a)pyrene adsorption kinetics.

As shown in Figures 8–11, all hybrid  $(\text{TiO}_2)_{100}(\text{O}_3\text{P-R})$  nanomaterials demonstrated remarkable 100% of removal efficiency of all 16 PAHs after 24 h. Such results confirmed that an aromatic function was not necessary to have efficient charge transfer, as reported by Bloom et al [9].

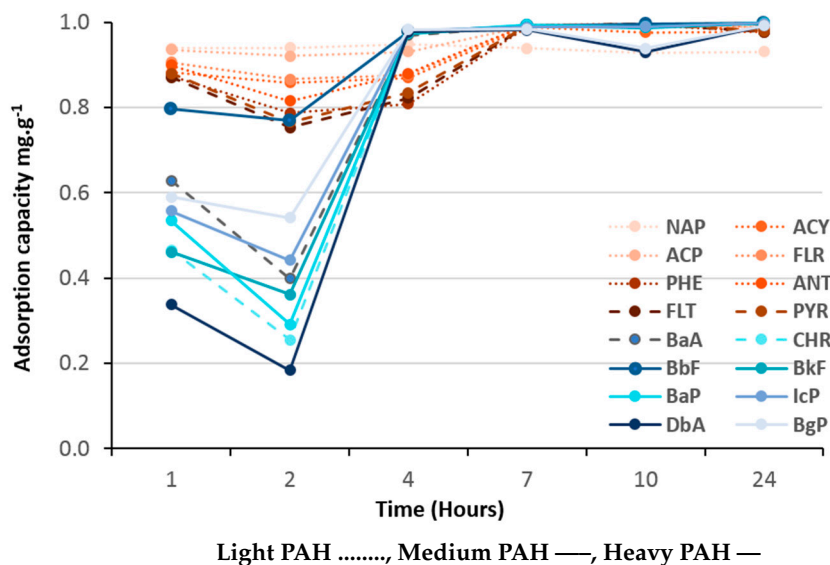


Figure 8. Adsorption kinetics of 16 PAHs on  $(TiO_2)_{100}(VPA)$ .

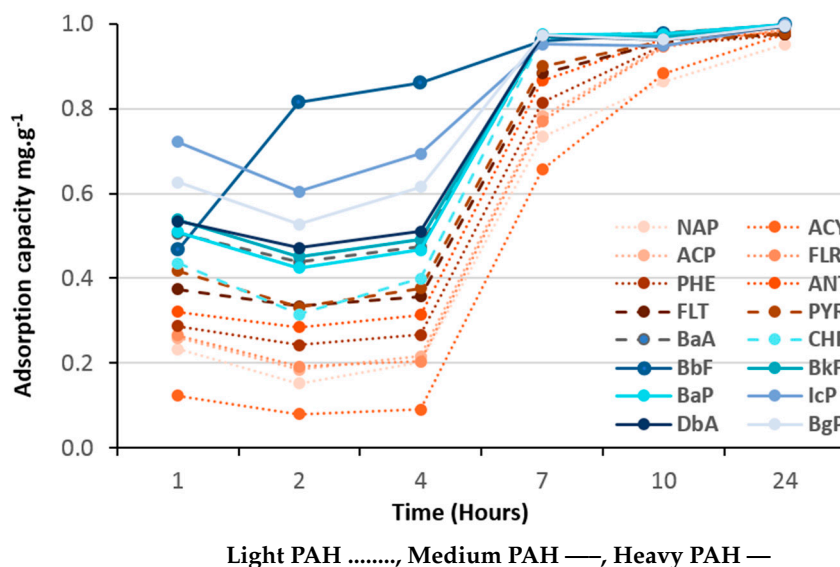


Figure 9. Adsorption kinetics of 16 PAHs on  $(TiO_2)_{100}(PPA)$ .

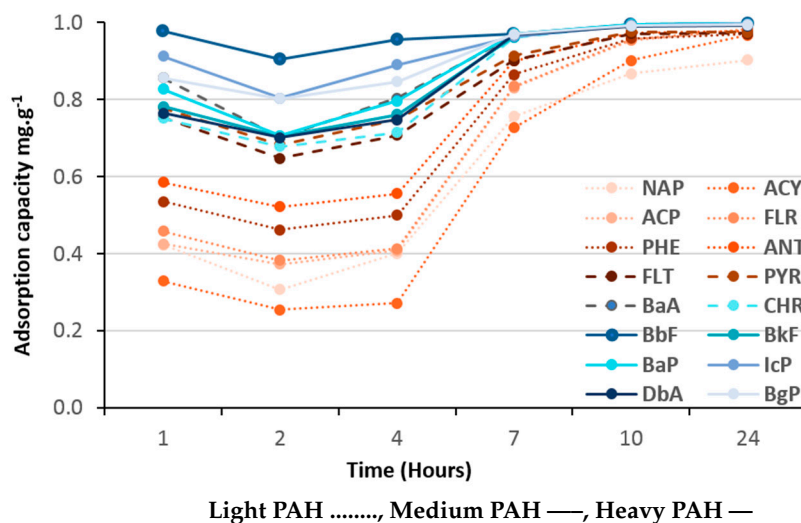
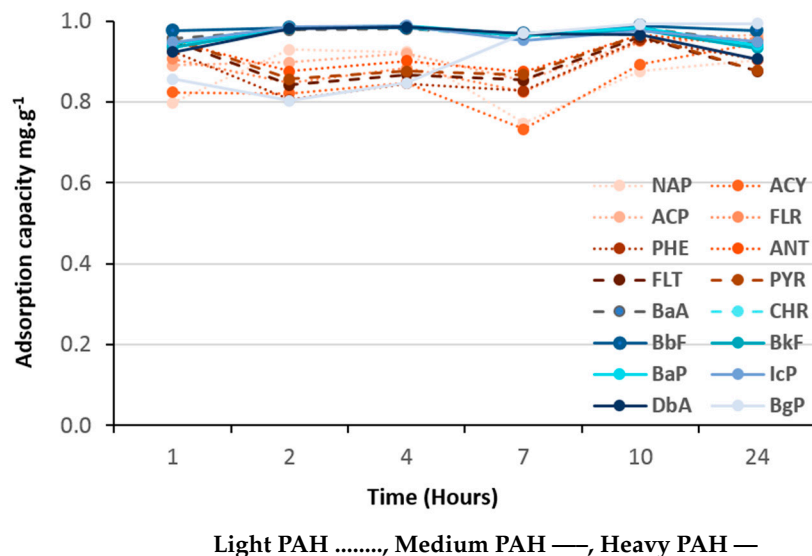


Figure 10. Adsorption kinetics of 16 PAHs on  $(TiO_2)_{100}(NMAPA)$ .



**Figure 11.** Adsorption kinetics of 16 PAHs on  $(\text{TiO}_2)_{100}(\text{HQPA})$ .

Adsorption kinetics of VPA-, PPA- and NMAPA-based material followed similar and two-stage patterns with first one ascribed as a competition between light, medium and heavy PAHs followed by an equilibrium one to reach 100% of adsorption of all PAHs. Interestingly, while VPA-based (vinyl) nanomaterial had more affinity with light PAH molecules in the first seven hours, going through PPA (phenyl) to NMAPA (naphtyl) gave totally opposite adsorption kinetic behaviors. In particular the NMAPA-based ligand displayed the highest affinity for the heavy PAHs during the first hours of experiment. We could ascribe this result to strongest quadrupole interactions between naphtyl groups (two cycles) and PAHs with several aromatic cycles than vinyl ones. It was also well-known that the most stable conformations of benzene dimers are parallel displaced or T-shaped compared to sandwich one [24]. One could speculate that these conformations led to different steric hindrance at the surface of the nano-materials and time was mandatory to reach different supramolecular assembly organizations. Other parameter that could be taken into account was the change of the adsorbent texture since PPA-and NMAPA-based mesoporous materials exhibited type H3 hysteresis loops consisting in the presence of macroporosity (more convenient for the diffusion of heavy PAHs) while VPA one exhibited type H2(b) hysteresis loop revealing small pore neck diameters (cavitation and pore blocking effects) [20]. We have already reported how supramolecular spatial arrangement of hybrid titania nanocrystals through the use of bi-functional ligands (DTPA) enabled to reach efficient lanthanide ionic separation with very high selectivity (i.e.,  $S_{\text{La}/\text{Gd}} = 160$ ) [25].

Finally,  $(\text{TiO}_2)_{100}(\text{HQPA})$  sample has shown more affinity to heavy PAH but did not exhibit any competition process during the first hours, adsorption percentages of all PAH being constant all over the experiment (Figure 11). In comparison with the PPA-based sample containing also one phenyl ring, this last result demonstrated that subtle change of the phenyl 3D spatial organization and/or texture [from H3 to H2(b) hysteresis loop] might drastically impact the selectivity of our hybrid nano-absorbents towards mixture of PAHs.

Thermodynamic studies and computational calculations are now under progress in order to elucidate whether mono or multilayer or T-shaped or parallel displaced conformations could be at the origin of such selectivity performances.

### 3. Experimental Section

#### 3.1. General Information

All manipulations have been carried out under an argon atmosphere using standard Schlenk and glovebox techniques. THF and HOiPr were dried using either an MBRAUN SPS-800 system

(Garching, Germany) (THF) or distillation over  $[\text{Al}(\text{OiPr})_3]_4$ , respectively. Deuterated solvents ( $\text{CDCl}_3$ , MeOD) were stored over molecular sieves. Vinyl phosphonic acid (VPA), phenyl phosphonic acid (PPA) and ammonium salt ( $\text{NnBu}_4\text{Br}$ ) were purchased from Sigma Aldrich (Saint-Louis, MO, USA) and were used as received. Phosphonic acids such as  $(\text{C}_{10}\text{H}_7)\text{CH}_2\text{NHCH}_2\text{CH}_2\text{PO}(\text{OH})_2$  (NMAPA),  $(\text{C}_9\text{H}_{10}\text{N})\text{CH}_2\text{CH}_2\text{PO}(\text{OH})_2$  (HQPA) were synthesized according to the published procedure and stored under argon [26].  $\text{Ti}(\text{OiPr})_4$  (TTIP) was purchased from Sigma Aldrich and distilled under vacuum prior used. The standard stock solution containing sixteen US-EPA PAHs at a concentration of 500 ppm each was purchased from Sigma Aldrich. It was diluted to a concentration of 200 ppb ( $\mu\text{g L}^{-1}$ ) each in deionized water: ethanol mixture prior used in extraction tests.

### 3.2. Product Characterizations

$^1\text{H}$  liquid and  $^{13}\text{C}$  solid state MAS NMR spectra were recorded on an AM-250 spectrometer Bruker (Billerica, MA, USA).  $^{31}\text{P}$  solid state MAS NMR were recorded on a Bruker DSX400 spectrometer spectra with a 4 mm probe and rotation speeds of 5 to 10 Kz. Analytical data were obtained from the Institut des Sciences Analytique (UMR 5280, Villeurbanne, France) by ICP. FT-IR spectra were recorded as Nujol suspensions (for air sensitive derivatives) or as KBr pellets (for hydrolyzed powders) on a Bruker Vector 22 FT-IR spectrometer at room temperature and registered from 4000 to  $400\text{ cm}^{-1}$ . DRIFT experiments were carried out on a Nicolet 6700 FTIR spectrophotometer (Thermo Fischer, Waltham, MA, USA) equipped with a MCT detector (number of scan: 64, resolution:  $4\text{ cm}^{-1}$ ). The recording mode was diffuse reflectance and the optical unit, Praying Mantis (Harrick). TGA/TDA data were collected with a model 92 system (Setaram, Lyon, France) in air with a thermal ramp of  $10\text{ }^\circ\text{C min}^{-1}$ . Powder X-ray diffraction data were obtained with a D5005 diffractometer (Siemens, Munich, Germany) by using  $\text{Cu-K}\alpha$  radiation at the scan rate of  $0.02^\circ 2\theta\text{ s}^{-1}$  with step times of 1 and 16 s for routine or for expanded region spectra, respectively. BET experiments were carried out with an ASAP 2010 system after the samples were desorbed at  $100\text{ }^\circ\text{C}$  for 6 h.

### 3.3. Synthesis of Titanium Precursors

#### 3.3.1. Synthesis of $[\text{Ti}_2(\text{OiPr})_6(\text{O}_3\text{PC}_2\text{H}_3)]_m$ (1)

Under an argon atmosphere  $\text{Ti}(\text{OiPr})_4$  (1.48 mL, 4.9 mmol) was dissolved in anhydrous THF (10 mL). In another Schlenck flask,  $\text{CH}_2=\text{CH-PO}(\text{OH})_2$  (272 mg, 2.5 mmol) was added to anhydrous THF (23 mL). Under an inert atmosphere, the vinyl phosphonic acid solution was added dropwise to the  $\text{Ti}(\text{OiPr})_4$  one. The mixture was stirred at room temperature for 18 h. After evaporation of the solvent, 1.62 g (quantitative yield relative to titanium) of **1**, soluble in THF, were obtained as a brown oil. Anal. Calcd for  $\text{C}_{20}\text{H}_{45}\text{O}_9\text{PTi}_2$ : Ti: 17.20; P: 5.56; Found Ti: 17.24, P: 5.50.  $^1\text{H-NMR}$  ( $20\text{ }^\circ\text{C}$ ,  $\text{CDCl}_3$ );  $\delta$  ppm 6.25–5.70 (m, 3H,  $-\text{CH}=\text{CH}_2$ ); 5.05–4.30 (m, 6H,  $-\text{OCH}$ ); 1.45–1.06 (m, 36H,  $-\text{CH}_3$ ).  $^{31}\text{P}\{^1\text{H}\}\text{-NMR}$  ( $20\text{ }^\circ\text{C}$ ,  $\text{CDCl}_3$ );  $\delta$  ppm: 7.46. FT-IR (Nujol),  $\text{cm}^{-1}$ : 510 (s), 616 (s), 710 (m), 748 (m), 797(s), 851 (m) ( $\nu$  Ti–O); 955 (s), 1008 (vs), 1056 (s), 1082 (s) ( $\nu$  P–O); 1126 (vs), 1151 (sh), 1179 (sh) ( $\nu$  C–O); 1261 (m) ( $\nu$  P=O); 1331 (w); 1615(w) ( $\nu$  C=C).

#### 3.3.2. Synthesis of $[\text{Ti}_2(\text{OiPr})_6(\text{O}_3\text{PC}_6\text{H}_5)]_m$ (2)

Using the same procedure as previously described but with  $\text{Ti}(\text{OiPr})_4$  (1.51 mL, 5 mmol) dissolved in anhydrous THF (6 mL) and  $\text{C}_6\text{H}_5\text{PO}(\text{OH})_2$  (395 mg, 2.5 mmol) in anhydrous THF (17 mL) gave 1.76 g (quantitative yield relative to titanium) of **2** as a light brown oil soluble in THF. Anal. Calcd for  $\text{C}_{24}\text{H}_{47}\text{O}_9\text{PTi}_2$ : Ti: 15.79, P: 5.11; Found Ti: 15.82, P: 5.13.  $^1\text{H-NMR}$  ( $20\text{ }^\circ\text{C}$ ,  $\text{CDCl}_3$ );  $\delta$  ppm: 7.90–6.80 (m, 5H,  $-\text{C}_6\text{H}_5$ ); 5.14–4.23 (m, 6H,  $-\text{OCH}$ ); 1.45–1.06 (m, 36H,  $-\text{CH}_3$ ).  $^{31}\text{P}\{^1\text{H}\}\text{-NMR}$  ( $20\text{ }^\circ\text{C}$ ,  $\text{CDCl}_3$ );  $\delta$  ppm: 9.70. FT-IR (Nujol),  $\text{cm}^{-1}$ : 612(m), 625 (m), 702 (m), 748 (m), 838 (m), 853 (m) ( $\nu$  Ti–O); 957 (s), 976 (s), 1009 (vs), 1034 (m), 1089 (s) ( $\nu$  P–O); 1135 (vs), 1162 (sh) ( $\nu$  C–O); 1257 (m) ( $\nu$  P=O); 1320 (w); 1630 (w) ( $\nu$  C=C).

### 3.3.3. Synthesis of $[\text{Ti}_2(\text{OiPr})_6(\text{O}_3\text{PCH}_2\text{CH}_2\text{NHCH}_2(\text{C}_{10}\text{H}_7))]_m$ (**3**)

Using the same procedure as previously described with  $(\text{C}_{10}\text{H}_7)\text{CH}_2\text{NHCH}_2\text{CH}_2\text{PO}(\text{OH})_2$  (0.290 g, 1 mmol) dissolved in hot isopropanol (20 mL) and  $\text{Ti}(\text{OiPr})_4$  (0.268 g, 2 mmol) in isopropanol (3 mL) under reflux for 8 h gave 0.83 g (quantitative yield relative to titanium) of **3** as an orange oil soluble in isopropanol under reflux and insoluble in THF. Anal. Calcd for  $\text{C}_{31}\text{H}_{56}\text{NO}_9\text{PTi}_2$ : Ti: 12.94, P: 4.18; Found Ti: 12.97, P: 4.14.  $^1\text{H-NMR}$  (20 °C, MeOD);  $\delta$  ppm: 8.12 (m, 1H,  $-\text{C}_{10}\text{H}_7$ ); 7.97–7.12 (m, 6H,  $-\text{C}_{10}\text{H}_7$ ); 4.67–4.34 (m, 2H,  $-\text{NCH}_2$ ); 4.16–3.70 (m, 6H,  $-\text{OCH}$ ); 3.42 (d,  $J = 33.5$  Hz, 2H,  $-\text{CH}_2$ ); 2.04 (dd,  $J = 35.3; 28.3$  Hz, 2H,  $-\text{PCH}_2$ ); 1.38–0.64 (m, 36H,  $-\text{CH}_3$ ).  $^{31}\text{P}$   $\{^1\text{H}\}$ -NMR (20 °C, MeOD);  $\delta$  ppm: 7.57. FT-IR (Nujol),  $\text{cm}^{-1}$ : 614(m), 624 (m), 708 (m), 748 (m), 843 (m), 853 (m) ( $\nu$  Ti–O); 956 (s), 977 (s), 1008 (vs), 1045 (m), 1086 (s) ( $\nu$  P–O); 1125 (vs), 1162 (sh) ( $\nu$  C–O); 1256 (m) ( $\nu$  P=O); 1325 (w); 1631 (w) ( $\nu$  C=C).

### 3.3.4. Synthesis of $[\text{Ti}_2(\text{OiPr})_6(\text{O}_3\text{PCH}_2\text{CH}_2(\text{NC}_9\text{H}_{10}))]_m$ (**4**)

Using the same procedure as previously described with  $(\text{C}_9\text{H}_{10}\text{N})\text{CH}_2\text{CH}_2\text{PO}(\text{OH})_2$  (0.256 g, 1 mmol) in hot isopropanol (20 mL) and  $\text{Ti}(\text{OiPr})_4$  (0.268 g, 2 mmol) in isopropanol (3 mL) under reflux for 8 h gave 0.80 g (quantitative yield relative to titanium) of **4** as an orange oil soluble in isopropanol under reflux and not soluble in THF. Anal. Calcd for  $\text{C}_{29}\text{H}_{56}\text{NO}_9\text{PTi}_2$ : Ti: 13.84, P: 4.48; Found Ti: 13.78, P: 4.50.  $^1\text{H-NMR}$  (20 °C, MeOD);  $\delta$  ppm: 7.68–7.42 (m, 2H,  $\text{C}_6\text{H}_4$ ); 7.08 (dt,  $J = 11.8, 9.0$  Hz, 2H,  $\text{C}_6\text{H}_4$ ); 4.45 (d,  $J = 64.9$  Hz, 2H,  $-\text{CH}_2$ ); 4.24–3.75 (m, 6H,  $-\text{OCH}$ ); 3.74–3.32 (m, 6H,  $-\text{NCH}_2$ ); 2.26–1.81 (m, 2H,  $-\text{PCH}_2$ ); 1.63–0.77 (m, 36H,  $-\text{CH}_3$ ).  $^{31}\text{P}$   $\{^1\text{H}\}$ -NMR (20 °C, MeOD);  $\delta$  ppm: 8.53. FT-IR (Nujol),  $\text{cm}^{-1}$ : 616(m), 621 (m), 738 (m), 787 (m), 848 (m), 875 (m) ( $\nu$  Ti–O); 955 (m), 986 (m), 1010 (vs), 1034 (m), 1083 (s) ( $\nu$  P–O); 1125 (vs), 1160 (sh), 1186 (s) ( $\nu$  C–O); 1260 (m) ( $\nu$  P=O); 1330 (w); 1630 (w) ( $\nu$  C=C).

## 3.4. Synthesis of Hybrid Nanomaterials $(\text{TiO}_2)_x(\text{O}_3\text{P-R})$

### 3.4.1. Preparation of $(\text{TiO}_2)_x(\text{VPA})$ nanoparticles

A solution based on  $[\text{Ti}_2(\text{OiPr})_6(\text{O}_3\text{PC}_2\text{H}_3)]_m$  (**1**, 0.165 mmol) +  $y$  mmol of  $\text{Ti}(\text{OiPr})_4$  in THF (20 mL) was stirred for 15 min. The resulting clear solution was then injected directly using a cannula into an aqueous solution (100 mL) containing  $(y + 2)/10$  mmol of  $\text{N}(\text{nBu})_4\text{Br}$  and heated until reflux. A white precipitate was immediately formed. Reflux was maintained for 3 h. The medium was then cooled to room temperature, and the white solid formed was recovered by centrifugation (4000 rpm, 1 h) and then washed once with water (75 mL) and twice with ethanol ( $2 \times 75$  mL). The resulting white solids [denoted as  $(\text{TiO}_2)_x(\text{VPA})$ ] were dried at 70 °C for 18 h before characterization. Values of  $x$  were been fixed in order to get a series of hybrid  $\text{TiO}_2$  nanomaterials with Ti/P molar ratios ranging from 2 to 200 (Table 4). For comparison, the hydrolysis of pure  $[\text{Ti}_2(\text{OiPr})_6(\text{O}_3\text{PC}_2\text{H}_3)]_m$  (**1**) solution ( $y = 0$ ) was performed to produce a  $(\text{TiO}_2)_2(\text{VPA})$  sample.

**Table 4.** Ratios of Ti/P and amounts of **1**,  $[\text{Ti}_2(\text{OiPr})_6(\text{O}_3\text{PC}_2\text{H}_3)]_m$  and  $y$ ,  $\text{Ti}(\text{OiPr})_4$  aimed at their co-hydrolysis

Ti/P (Molar Ratio)	2	25	50	75	100	125	150	200
<b>1</b> (mmol)	6.711	0.165	0.165	0.165	0.165	0.165	0.165	0.165
<b>y</b> (mmol)	0.00	3.81	7.95	6.05	8.11	10.21	12.26	16.4

### 3.4.2. Preparation of $(\text{TiO}_2)_{100}(\text{PPA})$ Nanoparticles

The same procedure described below using  $[\text{Ti}_2(\text{OiPr})_6(\text{O}_3\text{PC}_6\text{H}_5)]_m$  (**2**, 0.207 mmol) and  $\text{Ti}(\text{OiPr})_4$  (10.143 mmol) afforded a white powder of  $(\text{TiO}_2)_{100}(\text{PPA})$ .  $^{31}\text{P}$ -MAS NMR: 19.15, 13.95 ppm. BET ( $\text{N}_2$ ):  $285 \text{ m}^2 \cdot \text{g}^{-1}$ .

### 3.4.3. Preparation of $(\text{TiO}_2)_{100}(\text{O}_3\text{P-R})$ Nanoparticles: $\text{R} = \text{CH}_2\text{CH}_2\text{NHCH}_2(\text{C}_{10}\text{H}_7)$ (NMAPA), $\text{CH}_2\text{CH}_2(\text{NC}_9\text{H}_{10})$ (HQPA)

A modified procedure as described below (replacing THF by hot isopropanol) was used starting from precursors **3** and **4** and about 10 mmol of  $\text{Ti}(\text{OiPr})_4$  to afford white powders of  $(\text{TiO}_2)_{100}(\text{O}_3\text{P-R})$ . The hybrid nanomaterials were characterized by solid state  $^{31}\text{P}$ -MAS NMR, powder XRD, BET, elemental analysis and TGA. Powder XRD: Anatase phase (average particle size = 5 nm).  $(\text{TiO}_2)_{100}(\text{NMAPA})$ :  $^{31}\text{P}$ -MAS NMR  $\delta$  ppm = 18.09; BET ( $\text{N}_2$ ):  $225 \text{ m}^2 \cdot \text{g}^{-1}$ .  $(\text{TiO}_2)_{100}(\text{HQPA})$ :  $^{31}\text{P}$ -MAS NMR  $\delta$  ppm = 18.24; BET ( $\text{N}_2$ ):  $322 \text{ m}^2 \cdot \text{g}^{-1}$ .

### 3.5. PAH Batch Adsorption Test Procedure

For all tests, a 200 ppb PAH solution was prepared by diluting in a water:ethanol (24:1) mixture 4 mL of a 500 ppm standard solution containing the US-EPA PAHs (the weight concentration of the 16 PAHs being equal in the standard stock solution). The adsorption tests were made using 10 mg of each solid material under stirring at 20 °C in 50 or 100 mL of PAH aqueous solution. Samples of 12 mL were collected after 1, 2, 4, 7, 10 and 24 h, centrifuged and 10 mL were analyzed by SPE using commercial strata-X  $\text{C}_{18}$  cartridges to extract non-adsorbed PAHs. The elution of the adsorbed compounds was carried out by passing 3 mL of ethyl acetate. The extract was concentrated at 40 °C under a stream of nitrogen to a final volume of 200  $\mu\text{L}$ . The eluates were analyzed by GC-ToF in SIM mode on a DB-5MS UI column (30 m  $\times$  0.25 mm I.D, thickness 0.25  $\mu\text{m}$ ) with helium as carrier gas. The injection was performed in splitless mode (1  $\mu\text{L}$ ) at a temperature of 300 °C. The heating gradient was: 60 °C (1 min) at 320 °C (25 °C/min), 32 °C for 10 min.

## 4. Conclusions

In conclusion, a robust sol-gel process, starting from novel heteroleptic titane phosphonate-alkoxides precursors, was developed in order to tune finely the surface functionalization of nanocrystallites of titania with phosphonate ligand (PA). Series of hybrid nanomaterials bearing different amount and nature of unsaturated groups (vinyl, phenyl, naphthyl) were elaborated and thoroughly characterized. Their performances as nano-adsorbents through  $\pi$ - $\pi$  stacking demonstrated remarkable removal efficiencies of 100% over a mixture of 16 PAHs (listed by the U.S. Environmental Protection Agency). The adsorption kinetics results have shown that systems with a ratio  $\text{TiO}_2/\text{PA} = 100$  reached the equilibrium after 24 h and high adsorption capacities of around  $1 \text{ mg} \cdot \text{g}^{-1}$  per PAH were found. The selectivity of PAH sorption process depended on the nature of the unsaturated-based phosphonate ligands, on the self-agglomeration of the surface-functionalized nano-particles and on the textures of the nanomaterials. Hence, mesoporous vinyl-based titania nanomaterials have demonstrated high affinity for light PAHs while macro-, mesoporous phenyl-based one had high affinity for heavy PAHs. Such findings would be very helpful in identifying factors affecting selective PAHs remediation from aqueous media in the presence of competing species (PCB, diclofenac) or PAH mixtures.

**Supplementary Materials:** The supplementary materials are available online.

**Author Contributions:** Conceptualization, S.D. and N.B.O.; Methodology, S.D. and N.B.O.; Validation, S.D., N.B.O. and Q.A.T.; Formal Analysis, N.B.O. and Q.A.T.; Investigation, S.D., N.B.O. and Q.A.T.; Data Curation, S.D., N.B.O. and Q.A.T.; Writing-Original Draft Preparation, N.B.O.; Writing-Review & Editing, S.D. and N.B.O.; Supervision, S.D.; Project Administration, S.D.; Funding Acquisition, S.D.

**Funding:** The authors acknowledge the Region Rhône-Alpes for financial support (ADR 2009-contract n° 1101538402).

**Acknowledgments:** The authors thank Laure WIEST, Cédric FRATTA and Emmanuelle VUILLET from Institut des Sciences Analytiques (Villeurbanne, UMR 5280), Chantal LORENTZ from IRCELYON (Villeurbanne, UMR 5256) and Kai Chung SZETO from LCOMS/C2P2 laboratory (Villeurbanne, UMR 5265) for carrying out CG-ToF, multinuclear MAS NMR and DRIFT experiments, respectively.

**Conflicts of Interest:** The authors declare no conflict of interest.

## References

1. Shuttleworth, K.L.; Cerniglia, E. Environmental aspects of PAH biodegradation. *Appl. Biochem. Biotech.* **1995**, *54*, 291–302. [[CrossRef](#)]
2. Pashin, Y.V.; Bakhitova, L.M. Mutagenic and carcinogenic properties of polycyclic aromatic hydrocarbons. *Environ. Health Perspect.* **1979**, *30*, 185–189. [[CrossRef](#)] [[PubMed](#)]
3. Rubio-Clemente, A.; Torres-Palma, R.A.; Peñuela, G.A. Removal of polycyclic aromatic hydrocarbons in aqueous environment by chemical treatments: A review. *Sci. Total Environ.* **2014**, *478*, 201–225. [[CrossRef](#)] [[PubMed](#)]
4. Ncube, S.; Madikizela, L.; Cukrowska, E.; Chimuka, L. Recent advances in the adsorbents for isolation of polycyclic aromatic hydrocarbons (PAHs) from environmental sample solutions. *TrAC-Trend Anal. Chem.* **2018**, *99*, 101–116. [[CrossRef](#)]
5. Lamichhane, S.; Bal Krishna, K.C.; Sarukkalige, R.; Lamichhane, S.; Bal Krishna, K.C.; Sarukkalige, R. Polycyclic aromatic hydrocarbons (PAHs) removal by sorption: A review. *Chemosphere* **2016**, *148*, 336–353. [[CrossRef](#)] [[PubMed](#)]
6. Liu, Z.; Li, Q.; Wu, Q.; Kuo, D.T.F.; Chen, S.; Hu, X.; Deng, M.; Zhang, H.; Luo, M. Removal efficiency and risk assessment of polycyclic aromatic hydrocarbons in a typical municipal wastewater treatment facility in Guangzhou, China. *Int. J. Environ. Res. Public Health* **2017**, *14*, 861. [[CrossRef](#)] [[PubMed](#)]
7. Dougherty, D.A. The Cation– $\pi$  Interaction. *Acc. Chem. Res.* **2013**, *46*, 885–893. [[CrossRef](#)] [[PubMed](#)]
8. Janiak, C.; Janiak, C. A critical account on  $\pi$ – $\pi$  stacking in metal complexes with aromatic nitrogen-containing ligands†. *J. Chem. Soc. Dalton* **2000**, *21*, 3885–3896. [[CrossRef](#)]
9. Bloom, J.W.G.; Wheeler, S.E. Taking the aromaticity out of aromatic interactions. *Angew. Chem. Int. Ed.* **2011**, *123*, 7993–7995. [[CrossRef](#)]
10. Jurado-Sánchez, B.; Wang, J. Micromotors for environmental applications: A review. *Environ. Sci. Nano* **2018**, *7*. [[CrossRef](#)]
11. Mutin, P.H.; Guerrero, G.; Vioux, A.; Mutin, P.H.; Guerrero, G.; Vioux, A. Hybrid materials from organophosphorus coupling molecules. *J. Mater. Chem.* **2005**, *15*, 3761. [[CrossRef](#)]
12. Guerrero, G.; Alauzun, J.G.; Granier, M.; Laurencin, D.; Mutin, P.H.; Guerrero, G.; Alauzun, J.G.; Granier, M.; Laurencin, D.; Mutin, P.H. Phosphonate coupling molecules for the control of surface/interface properties and the synthesis of nanomaterials. *Dalton T.* **2013**, *42*, 12569. [[CrossRef](#)] [[PubMed](#)]
13. Smith, J.A.; Jaffé, P.R.; Chiou, C.T. Effect of Ten Quaternary Ammonium Cations on Tetrachloromethane Sorption to Clay from Water. *Environ. Sci. Technol.* **1990**, *24*, 1167–1172. [[CrossRef](#)]
14. Goutailler, G.; Guillard, C.; Daniele, S.; Hubert-Pfalzgraf, L.G. Low temperature and aqueous sol-gel deposit of photocatalytic active nanoparticulate TiO<sub>2</sub>. *J. Mater. Chem.* **2002**, *13*, 342–346. [[CrossRef](#)]
15. Thommes, M.; Kaneko, K.; Neimark, A.V.; Olivier, J.P.; Rodriguez-Reinoso, F.; Rouquerol, J.; Sing, K.S.W. Physisorption of gases, with special reference to the evaluation of surface area and pore size distribution (IUPAC Technical Report). *Pure Appl. Chem.* **2015**, *87*. [[CrossRef](#)]
16. Davidowski, S.K.; Holland, G.P. Solid-State NMR Characterization of Mixed Phosphonic Acid Ligand Binding and Organization on Silica Nanoparticles. *Langmuir* **2016**, *32*, 3253–3261. [[CrossRef](#)] [[PubMed](#)]
17. Bhandary, R.; Alauzun, J.G.; Hesemann, P.; Stocco, A. Phase transfer of TiO<sub>2</sub> nanoparticles from water to ionic liquid triggered by phosphonic acid grafting. *Soft Matter* **2017**, *13*, 8023–8026. [[CrossRef](#)] [[PubMed](#)]
18. Brodard-Severac, F.; Guerrero, G.; Maquet, J.; Florian, P.; Gervais, C.; Mutin, P.H. High-Field 17 O MAS NMR Investigation of Phosphonic Acid Monolayers on Titania. *Chem. Mater.* **2008**, *20*, 5191–5196. [[CrossRef](#)]
19. Liu, X.; Hu, Y.; Stellacci, F. Mixed-ligand nanoparticles as supramolecular receptors. *Small* **2011**, *7*, 1961–1966. [[CrossRef](#)] [[PubMed](#)]
20. Cychosz, K.A.; Guillet-Nicolas, R.; García-Martínez, J.; Thommes, M. Recent advances in the textural characterization of hierarchically structured nanoporous materials. *Chem. Soc. Rev.* **2017**, *46*, 389–414. [[CrossRef](#)] [[PubMed](#)]
21. Balati, A.; Shahbazi, A.; Amini, M.M.; Hashemi, S.H. Adsorption of polycyclic aromatic hydrocarbons from wastewater by using silica-based organic–inorganic nanohybrid material. *J. Water Reuse Desalin.* **2015**, *5*, 50. [[CrossRef](#)]

22. Vidal, C.B.; Barros, A.L.; Moura, C.P.; de Lima, A.C.A.; Dias, F.S.; Vasconcellos, L.C.G.; Fachine, P.B.A.; Nascimento, R.F. Adsorption of polycyclic aromatic hydrocarbons from aqueous solutions by modified periodic mesoporous organosilica. *J. Colloid Interf. Sci.* **2011**, *357*, 466–473. [[CrossRef](#)] [[PubMed](#)]
23. Costa, J.A.S.; Garcia, A.C.F.S.; Santos, D.O.; Sarmiento, V.H.V.; de Mesquita, M.E.; Romão, L.P.C. Applications of inorganic–organic mesoporous materials constructed by self-assembly processes for removal of benzo[k]fluoranthene and benzo[b]fluoranthene. *J. Sol.-Gel Sci. Technol.* **2015**, *75*, 495–507. [[CrossRef](#)]
24. DiStasio, R.A.; von Helden, G.; Steele, R.P.; Head-Gordon, M. On the T-shaped structures of the benzene dimer. *Chem. Phys. Lett.* **2007**, *437*, 277–283. [[CrossRef](#)]
25. Rahal, R.; Annani, F.; Pellet-Rostaing, S.; Arrachart, G.; Daniele, S. Surface modification of titanium oxide nanoparticles with chelating molecules: New recognition devices for controlling the selectivity towards lanthanides ionic separation. *Sep. Purif. Technol.* **2015**, *147*, 220–226. [[CrossRef](#)]
26. Bou Orm, N.; Dkhissi, Y.; Daniele, S.; Djakovitch, L.; Bou Orm, N.; Dkhissi, Y.; Daniele, S.; Djakovitch, L. Synthesis of 2-(arylamino)ethyl phosphonic acids via the aza-Michael addition on diethyl vinylphosphonate. *Tetrahedron* **2013**, *69*, 115–121. [[CrossRef](#)]

**Sample Availability:** Samples of the compounds are not available from the authors.



© 2018 by the authors. Licensee MDPI, Basel, Switzerland. This article is an open access article distributed under the terms and conditions of the Creative Commons Attribution (CC BY) license (<http://creativecommons.org/licenses/by/4.0/>).